ELEVATED TEMPERATURE CRACK GROWTH*

K.S. Kim, R.H. Van Stone, S.N. Malik, and J.H. Laflen
General Electric Aircraft Engines
Cincinnati, Ohio

Critical gas turbine engine hot section components such as blades, vanes, and combustor liners tend to develop minute cracks during the early stages of operation. These cracks may then grow under conditions of fatigue and creep to critical size. Current methods of predicting growth rates or critical crack sizes are inadequate, which leaves only two extreme courses of action. The first is to take an optimistic view with the attendant risk of an excessive number of service failures. The second is to take a pessimistic view and accept an excessive number of "rejections for cause" at considerable expense in parts and down time. Clearly it is very desirable to develop reliable methods of predicting crack growth rates and critical crack sizes.

To develop such methods, it is desirable to relate the processes that control crack growth in the immediate vicinity of the crack tip to parameters that can be calculated from remote quantities, such as forces, stresses, or displacements. The most likely parameters appear to be certain path-independent (P-I) integrals, several of which have already been proposed for application to high temperature inelastic problems. A thorough analytical and experimental evaluation of these parameters needs to be made which would include elevated temperature isothermal and thermomechanical fatigue, both with and without thermal gradients.

In any investigation of fatigue crack growth, the role of crack closure should be addressed in order to develop the appropriate crack growth model. Analytically, this requires the use of gap elements in a nonlinear finite element code to predict closure loads. Such predictions must be verified experimentally through detailed measurements; the best method for measuring crack closure has not been established in previous studies.

It is the purpose of this contract (NAS3-23940) to determine the ability of currently available P-I integrals to correlate fatigue crack propagation under conditions that simulate the turbojet engine combustor liner environment. The utility of advanced fracture mechanics measurements will

also be evaluated and determined during the contract. To date, the bulk of the experimental data has been collected, and the final analytical effort is in progress. It has shown that the experimentally measured displacements and loads can be accurately predicted by finite element analyses that consider the growth of the fatigue crack. These results are being used to evaluate nonlinear fracture mechanics parameters for correlating the observed fatigue crack growth rates for different strain ranges. In previous years, the selection of Alloy 718, the specimen design and analysis, the review of the P-I integrals, and the analysis of a temperature gradient specimen test have been presented. This report will summarize only the work performed during the previous year. A final report will be released next year.

DATA ANALYSIS

During the past year, extensive analysis has been made of the isothermal and thermal mechanical fatigue (TMF) crack growth test data. The primary effort of this activity was to use the experimental results to set the boundary conditions for the finite element analyses. Also, this effort is providing a linear elastic fracture mechanics description of the data. The way in which the boundary conditions are derived will be illustrated using results for specimen N4-3, a buttonhead, single edge notch (SEN) specimen tested at 538C with a strain range of 1.15% and a strain R-ratio of -1.

BOUNDARY CONDITIONS FOR FINITE ELEMENT ANALYSIS

Figure 1 shows a schematic of the gage section of the buttonhead SEN specimen and the location of the three extensometers. It was found that the crack mouth opening displacement (CMOD) data clearly showed the cusping in the hysteresis loop, indicating the presence of crack closure. This test program was one of the first to simultaneously use different displacement measurements to detect closure. These data illustrated that the ability to detect closure was highly dependent on the location of the displacement measurement. Of the greatest significance was the apparent absence of cusping in the back face displacements. This may suggest that back face deflection is not a very sensitive technique to detect crack closure in a SEN specimen.

The points of crack closure (decreasing load) and crack opening (increasing load) were determined by numerically differentiating the data points of each CMOD hysteresis loop. When a cusp occurs, there should be a change in the slope of the load-CMOD curve and a discontinuity in the second

derivative of load and CMOD. Using a seven point sliding polynomial technique, the second derivative of load with respect to CMOD was calculated for both increasing and decreasing load situations. The point of the discontinuity was determined for both situations. Comparison of the loads at crack closure with the hysteresis loops showed that this corresponded to the cusps in the loops.

Figure 2 shows the variation of maximum load (X), minimum load (+), closure load (square), and opening load (triangle) with cycle number for Specimen N4-3. At the beginning of the test, the CMOD loop does not show much cusping and it is difficult to reliably detect the presence of closure. As the crack grows, it becomes easier to detect closure. This results in a large amount of scatter in the opening and closure loads early in the test.

The finite element analyses were performed in two stages. The first was to use the maximum and minimum deflection boundary conditions as two load cases per cycle. A node releasing technique was used to permit the crack to propagate across the entire specimen, releasing two nodes per cycle. The purpose of this analysis was to build up the history-dependent crack surface wake. The results of this analysis were stored off and used as the starting point of more detailed finite element analysis. The second stage analysis was done at two fixed crack lengths. Ten loading steps were introduced to predict the occurrence of crack closure and opening. The P-I integrals were computed for these loading steps.

It was previously determined that the boundary conditions for this specimen geometry are linear displacements along the positions of the control and back face extensometer contact (6.4 mm above and below the plane of the crack). The displacements are determined by extrapolation of the control and back face extensometer readings. During a given cycle, the degree of bending increases with increasing load and deflection, resulting in a variation in the slope of the specimen deflections within a cycle. Thus, the experimental data were used to select the boundary conditions for these more extensive cyclic analyses.

The boundary conditions for the coarser finite element analysis were determined by iterating between the available data points. The solid line in Figure 3 shows the variation in crack length (a) with cycle number. The crack length positions corresponding to the finite element node locations are shown as triangles. The cycle count at these positions was calculated by linear interpolation between the actual data points. In a similar fashion, the maximum and minimum deflections corresponding to the interpolated cycle number were also calculated. The interpolated values were used as the boundary conditions for the coarser finite element analysis. A similar interplolation was also performed for loads and CMOD. These values were compared to those calculated from the finite element analysis.

Two crack lengths were selected from each test specimen to perform the more extensive cyclic analysis. Based on the crack growth rate data, the crack lengths of 0.95 and 2.54 mm were selected to provide a significant difference in crack length, bending strain, and crack growth rates. A total of 40 boundary conditions were obtained to describe the strain cycle for both crack lengths. These conditions were determined by placing a load case at maximum and minimum deflection, crack closure deflection, and crack opening deflection. Nine other load cases were placed between each of the following:

1. minimum and crack opening deflection

2. crack opening and maximum deflection

3. maximum and crack closure deflection

4. crack closure and minimum deflection

The load case positions were separated by a constant amount of CMOD within each of the four segments listed above. This is shown schematically in Figure 4 where the closed points indicate the four end points mentioned above. In the finite element analysis, 10 load cases were selected from the total set of 40.

This procedure was performed for the cycles on each side of the desired crack lengths. As in the case of the coarser boundary conditions, a linear interpolation was performed between the two experimental hysteresis loops. The remote displacements were reported at the same positions in the hysteresis loops.

FINITE ELEMENT RESULTS

Finite element simulations of crack growth at 538C were done for three ranges of strain: 0.5%, 1.15%, and 1.7%. These analyses used the GE-AE finite element code called CYANIDE. The crack was propagated from the initial length 0.32 mm to 2.54 mm with increments of 0.32 mm at each tensile peak. The computed and experimental loads were compared at the tensile and compressive peaks at different crack lengths. The correlations were very good for all three cases. The CMOD was also examined at different crack lengths, and a good agreement was again found between the analysis and test. The load versus crack length and the CMOD versus crack length plots are given in Figure 5 and Figure 6, respectively, for the medium strain range. The crack closure and opening analysis was made at two crack lengths (0.95 mm and 2.54 mm). The nominal stress (load/cross-sectional area) versus CMOD loops were plotted for all the cases, and they were compared with test results. In general, the computed load-displacement loop agreed

well with the test loop except for a shift in the CMOD measure. The reason for this is currently under investigation, but it is believed to be related to the cracks growing in a stable shear mode. The analysis predicted the closure and opening points within acceptable accuracies. The predicted loops for the medium strain range are compared with the experimental data in Figures 7 and 8 for the two different crack lengths of 0.95 mm and 2.54 mm. In constructing these figures, the experimental data were shifted by a constant amount to agree with the analytical predictions at the minimum load point.

CONCLUSIONS

As in previous reports, the prior year efforts are showing excellent progress toward the contract objectives. The finite element and test correlations demonstrate that an excellent, well understood set of consistent data has been generated. These data should lead to understanding the growth of cracks under cyclic conditions in the inelastic range. Currently, efforts are being directed toward utilizing the finite element results to evaluate the correlative ability of current nonlinear fracture mechanics parameters.

Additionally, analysis will be completed of the TMF data, and a final report will be written during the coming year.
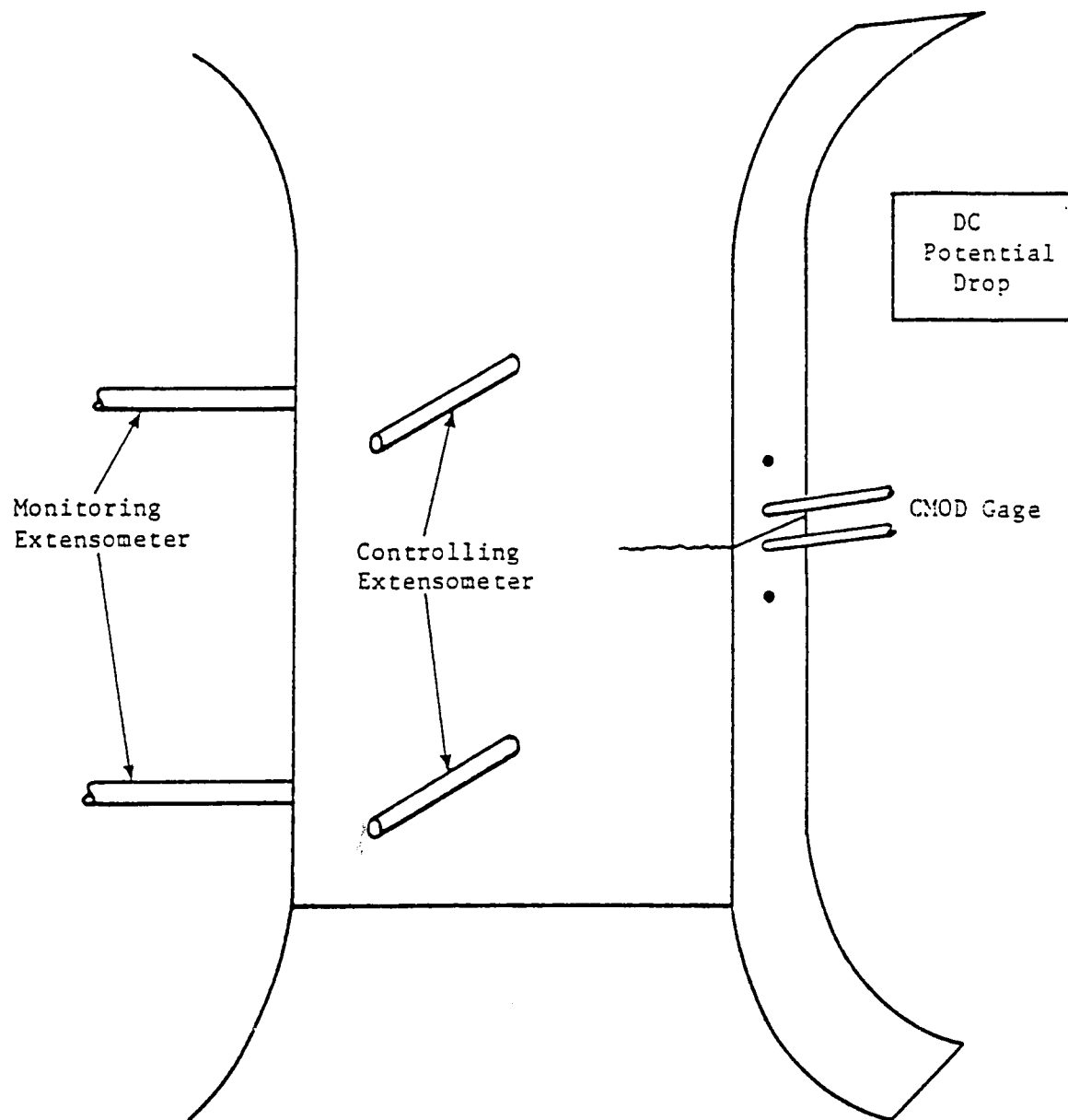
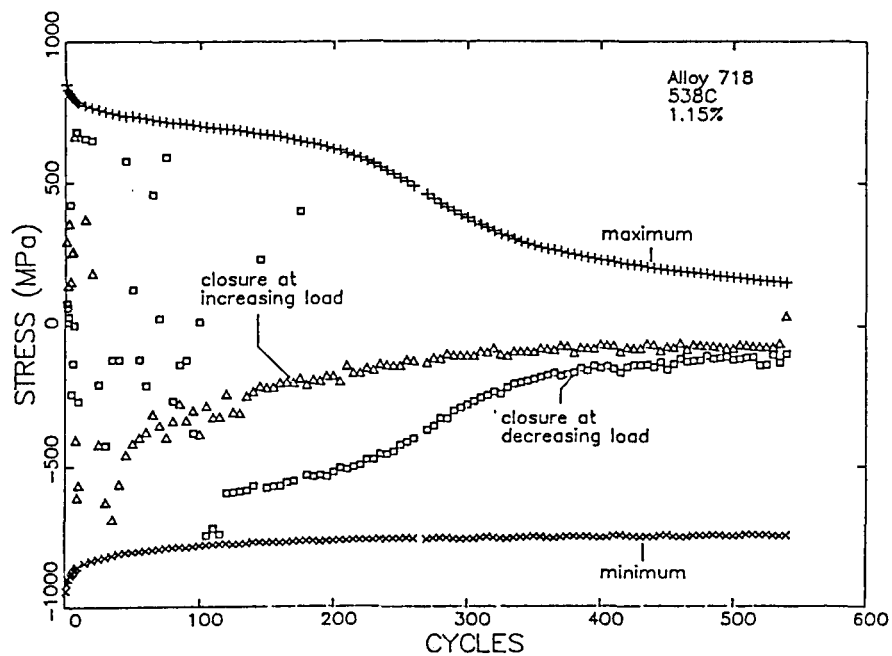Figure 1. Schematic Drawing of SEN Test Method.

Figure 2. Derived Closure Stress Points Compared to Maximum and Minimum Loads from Specimen N4-3
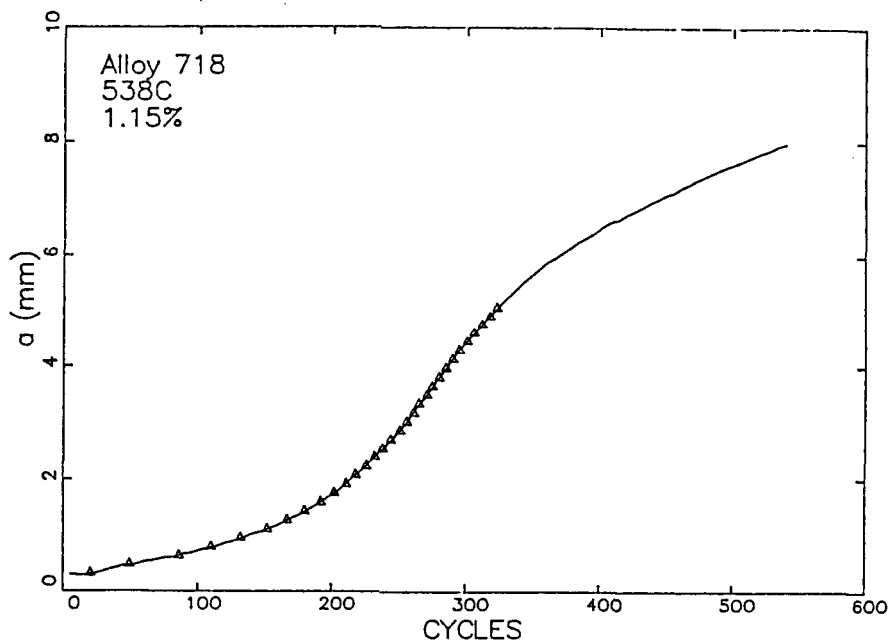

Figure 3. Crack Length Versus Cycles for Specimen N4-3.
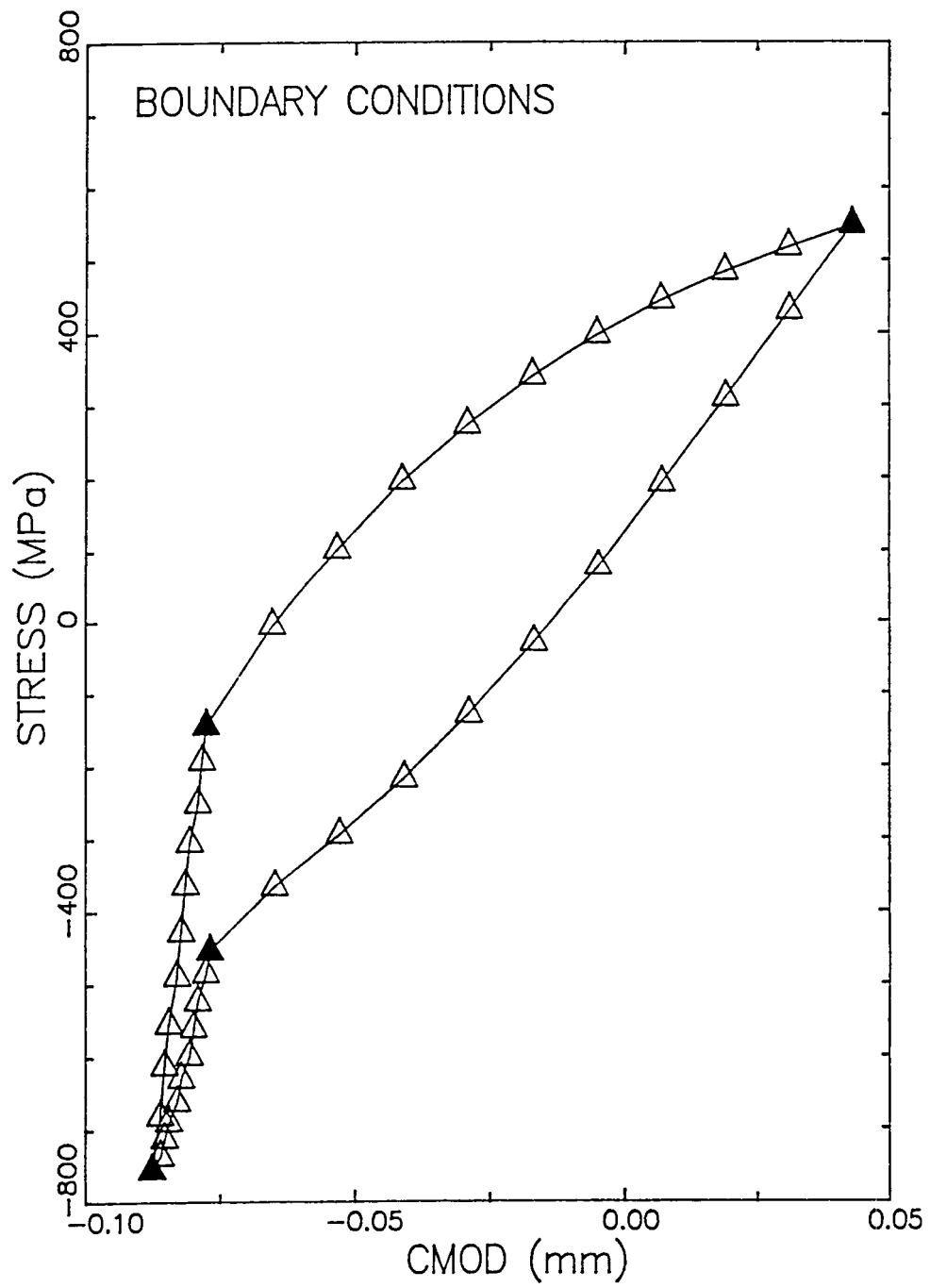The Symbols Show the Location of Finite Element Node Points.
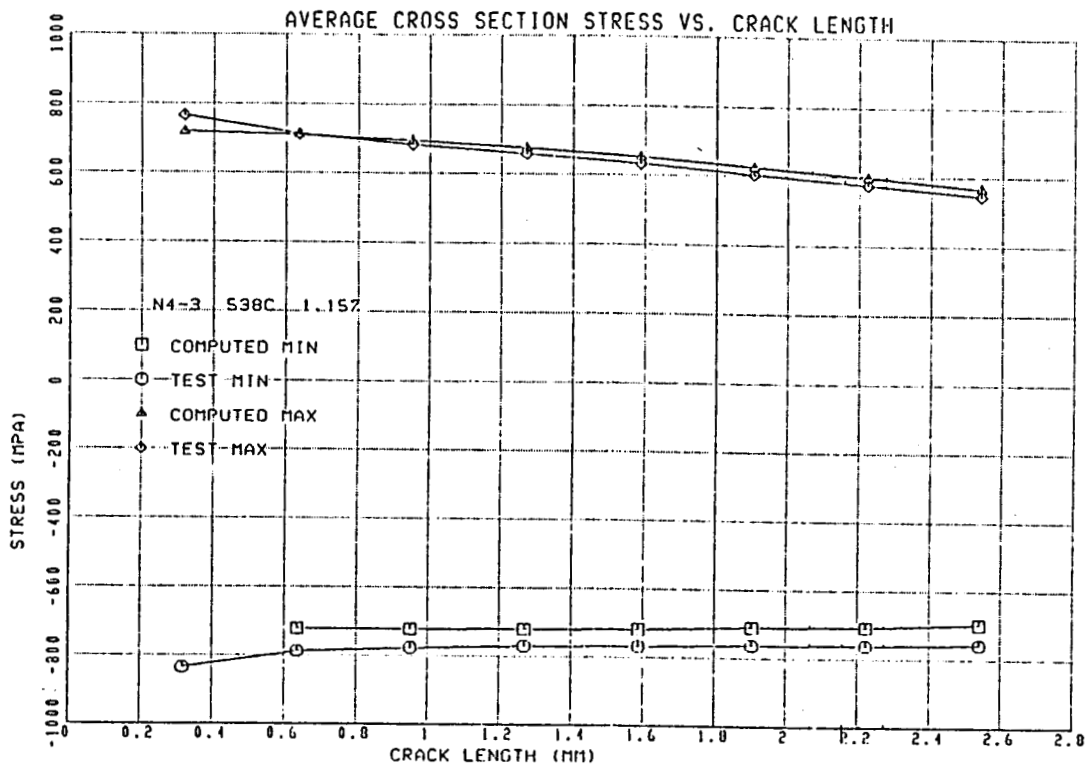
Figure 4. Selection of Boundary Conditions.

Figure 5. Predicted Stress As A Function of Crack Length - Coarse FEM
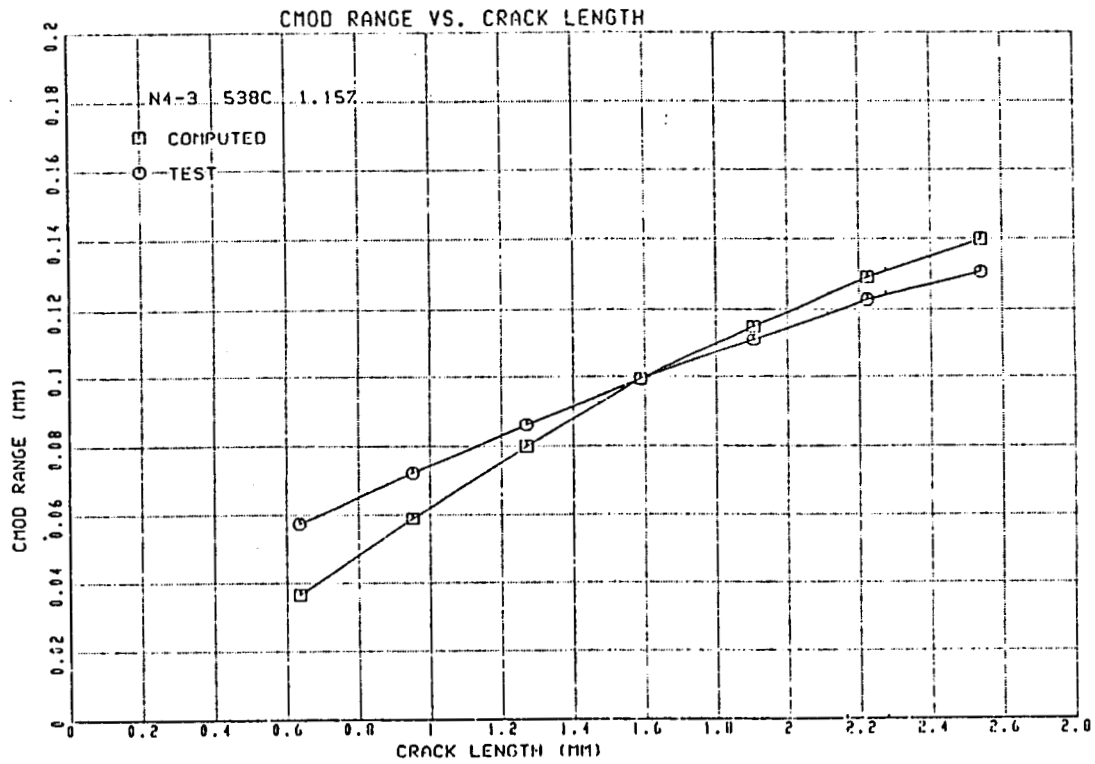

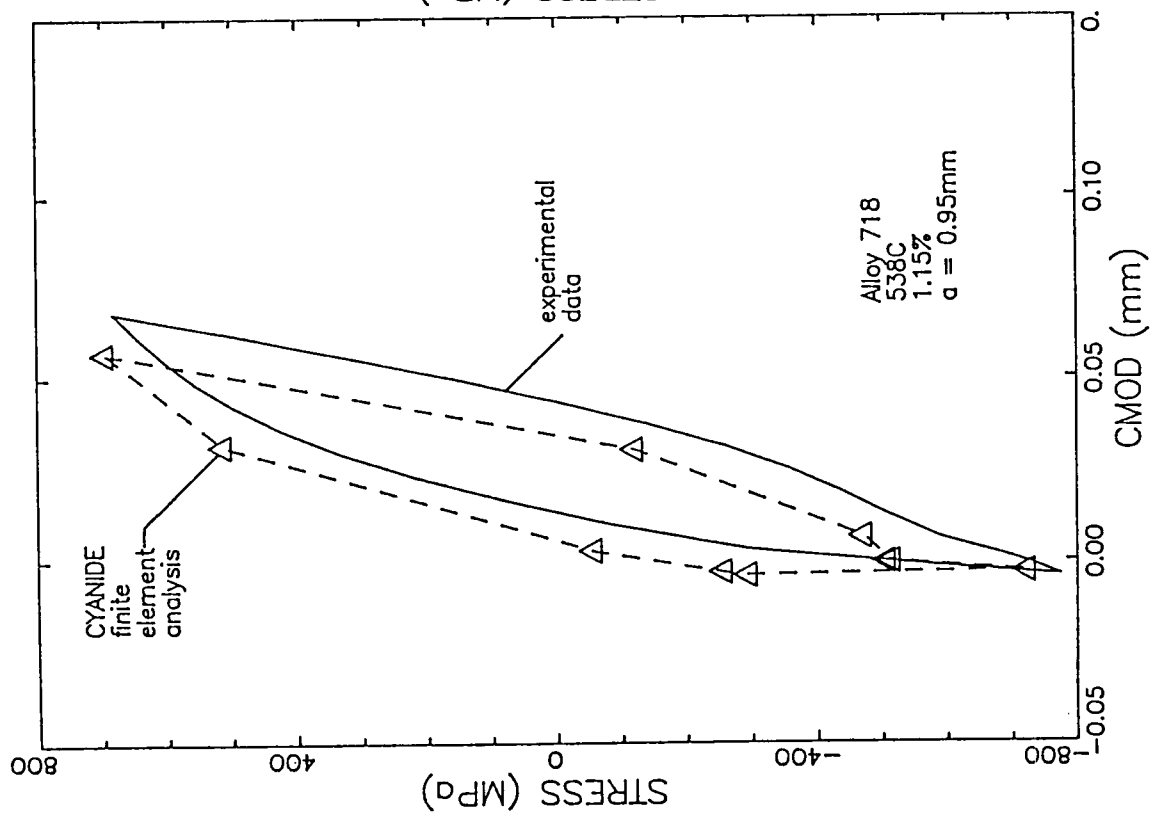Figure 6. Predicted CMOD Range Versus Crack Length - Coarse FEM
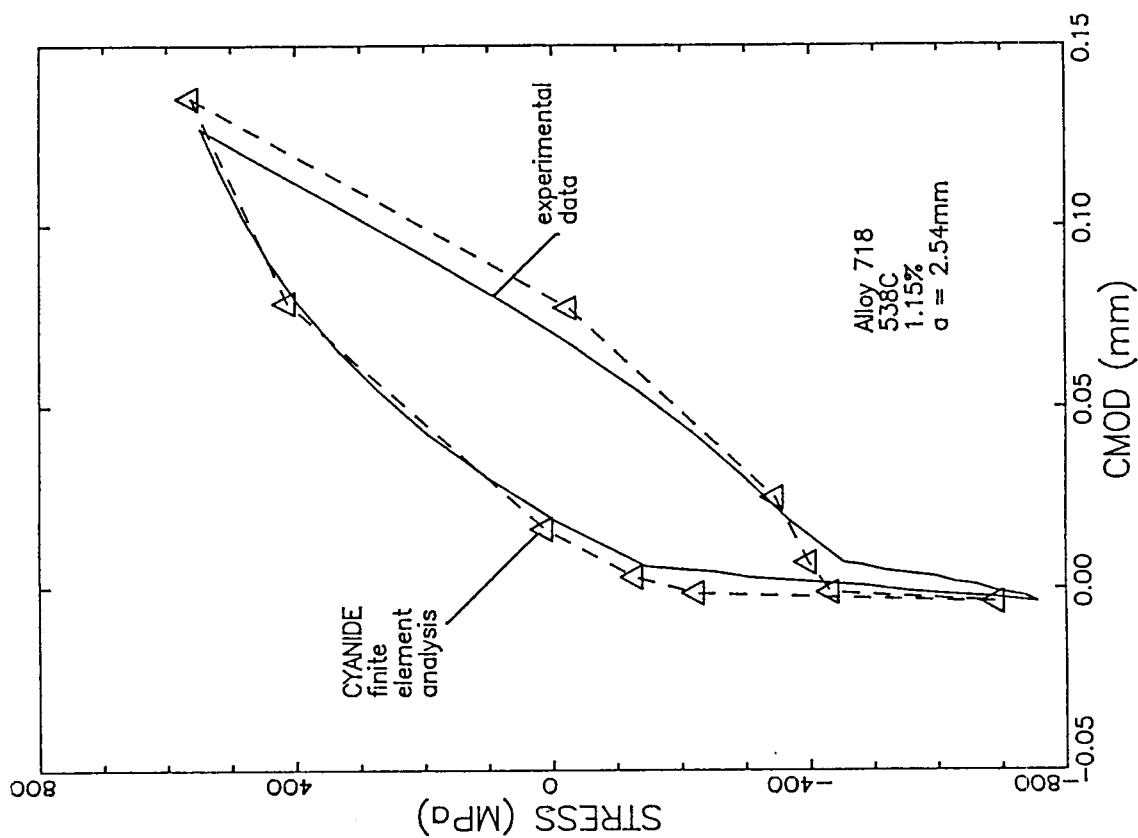
421

Figure 8. Comparison of Predicted and Experimentally Observed Stress-CMOD Hysteresis Loops for a Crack Length of 2.54 mm.

Figure 7. Comparison of Predicted and Experimentally Observed Stress-CMOD Hysteresis Loops for a Crack Length of 0.95 mm.